Biosensors and Bioelectronics 132 (2019) 343–351

Contents lists available at ScienceDirect

Biosensors and Bioelectronics

journal homepage: www.elsevier.com/locate/bios

Skin-inspired, open mesh electrochemical sensors for lactate and oxygen monitoring

Brandon K. Ashley[1], Matthew S. Brown[1], Youjoong Park, Sally Kuan, Ahyeon Koh*

Department of Biomedical Engineering, State University of New York at Binghamton, Binghamton, NY, USA

ARTICLE INFO

Keywords:
Deterministic geometries
Mechanically conformable
Porous
Wearable electronics
Lactate sensor
Oxygen sensor

ABSTRACT

Research in wearable electronics has paved the way for next-generation technology, sought to create point-of-care biosensors that combine chemical sensing on a biocompatible platform with a broad range of applications in human health monitoring. Despite significant progress, the microspatial mechanical mismatch and fluid-impermeable interface presented between skin and the electronics create adscititious problems in device lamination, conformality, and long-term monitoring. Herein, we engineered a skin-inspired, deterministically patterned, electrochemical biosensor that can be fully integrated with the curvilinear surface of the human body, while mechanically adapting to the natural stresses applied to the skin and allowing the mass transfer of gas and fluids. In particular, we developed mechanically-compliant lattice-structured biosensors for the continuous evaluation of lactate and oxygen. Systematic studies of the sensor performance were evaluated with variations in polymeric membranes and its ability to withstand commonplace harsh, multi-axial stresses.

1. Introduction

Recent advancements in biosensors and biomaterials can be attributed to the intuitive emulating of native architecture innate to the complex engineering of the human body (Fan et al., 2014; Jang et al., 2015; Jiang and Wang, 2016; Tang and Yin, 2017; Wang et al., 2018; Zhang, 2016). Interfacing electronics are a new class of wearable sensors that exhibit both mechanical and physical properties similar to the tissue of interest (Kim et al., 2012; Kim and Rogers, 2008). Designing sensors with the proper mechanical properties is crucial considering the potential mismatch between soft tissue and rigid electronics where incompatibility leads to decreased sensor performance, delamination, inflammation, and discomfort (Dickey, 2016; Hua et al., 2018; Rogers et al., 2010). Physically, non-porous devices prevent free fluid and gas diffusion, which limits sensor sensitivity and accuracy, increases inflammation, and disrupts the native dynamic physiochemical environment of the tissue (Brown et al., 2018; Rogers, 2017). Although advancements in the field are making great strides, there is a need for skin-inspired sensors that are bioinert, can emulate native tissue, and are compliant and porous. Achieving such results will act as a framework for providing real-time, accurate, precise, long-term biomarker monitoring for applications in physiological monitoring, multifunctional sensing, and health and fitness analysis (Liu et al., 2017; Yang and Gao, 2018).

Human skin is of interest as it is composed of anisotropic fibers (i.e., collagen and elastin) capable of adapting to compound multi-axial forces (Sacks and Sun, 2003), expressing viscoelastic properties, and nonlinear stress-strain dynamics (Flynn et al., 2011). Current biosensor technology challenges the fabrication of a device with mechanical properties similar to skin. Recent developments have transformed structures of intrinsically brittle materials into novel, soft electronics through innovative patterns, an advancement that allows rigid materials to exhibit stretchable characteristics (Wang et al., 2018). Stiff materials of once thin films can be translated into deterministic geometries: wavy (Fan et al., 2014), serpentine (Zhang et al., 2013), origami (Rogers et al., 2016), kirigami (Tang and Yin, 2017), crack (Liu et al., 2014), and interlocking (Ha et al., 2015) structures. Such remarkable strides can integrate and translate these novel structures into the same stretchable substrates that have been developed for on-skin electronics such as polymeric (Gao et al., 2016; Jeong et al., 2014; Kim et al., 2016; Liu et al., 2016; Matsuhisa et al., 2015), textile (Jang et al., 2014; Liu et al., 2015; Yoon et al., 2016), paper (Nie et al., 2010a, 2010b; Siegel et al., 2010), biodegradable materials (Hwang et al., 2012; Kang et al., 2016; Yu et al., 2016), and elastomeric materials (Dickey, 2016; Wang et al., 2018; Zhang, 2016). Current epidermal electronics can detect a wide range of

* Corresponding author.
E-mail address: akoh@binghamton.edu (A. Koh).
[1] Authors contributed equally to this work.

https://doi.org/10.1016/j.bios.2019.02.041
Received 27 November 2018; Received in revised form 19 February 2019; Accepted 20 February 2019
Available online 21 February 2019
0956-5663/

biomarkers including glucose (Bandodkar et al., 2015; Gao et al., 2016; Lee et al., 2016, 2017a), lactate (Gao et al., 2016; Imani et al., 2016), oxygen (Kim et al., 2016; Lochner et al., 2014; Luo et al., 2017), pH (Bandodkar et al., 2013; Yun et al., 2017), temperature (Hattori et al., 2014; Krishnan et al., 2017; Webb et al., 2013), pressure (Dagdeviren et al., 2014; Gong et al., 2014; Yao et al., 2013), and more. However, these devices are restricted by their fluid-impenetrable platforms, and lack of conformance to nonlinear, local skin mechanics despite having "soft" characteristics that limit their use in long-term monitoring and accuracy caused by local inflammation and biofluid accumulation (Brown et al., 2018; Dickey, 2016; Liu et al., 2017).

Skin-interfaced biosensors capable of exhibiting homologous mechanical properties and the interfaces that facilitate biofluid mass transfer will allow for accurate, real-time biomarker analysis. Clinically, such biomarker detection in blood, sweat, wound exudate, and tears holds significant potential in applications including chronic diseases, general health, and fitness monitoring, thereby eliminating costly and time-consuming laboratory testing (Brown et al., 2018; Heikenfeld et al., 2018; Koh et al., 2016; Liu et al., 2017). Therefore, there is great interest in developing soft, elastic devices that combine conformal contact, stretchability, porosity, and sensor performance that is indistinguishable from those on rigid, printable circuit boards (PCBs). These clinically relevant devices could be a vital tool in health diagnostics and monitoring.

Herein we present a skin-inspired, porous, elastic and conformable biosensor, engineered in deterministic geometries, capable of real-time biofluid monitoring. This innovative structure was inspired by Jang et al. (2015) and Ma et al. (2016), triangular unit structures allow for the device to be stretched in multiaxial directions. Augmentations were made to support biosensor function by incorporating repeating circular electrode units and encasing its electrochemical counterparts in a polyimide layer. The loose orientation of the triangular structures combined with the circular electrodes allows for a complex modulus response. Remarkably, we accomplished both electrochemical amperometric and enzymatic sensing with an ultrathin, porous, and skin-like platform. We produced lactate and oxygen electrochemical sensors capable of high-performance monitoring that have comparable mechanical elasticity and resilience to skin, and use a porous network to allow for passive, free fluid and gas diffusion for functional applications in biomedical devices.

2. Materials and methods

2.1. Materials

Sodium L-lactate, medium molecular weight chitosan, single-walled carbon nanotubes (SWCNT) in aqueous ink (2 mg/mL), toluene, 0% standard oxygen solution, iron(III) chloride ($FeCl_3$), potassium chloride (KCl), potassium ferricyanide ($K_3Fe(CN)_6$), Nafion (~5% in a mixture of lower aliphatic alcohols and water), and hydrogen chloride (HCl) were all purchased from Sigma Aldrich (St. Louis, MO). Sylgard 184 (i.e., polydimethylsiloxane (PDMS)) was purchased from Ellsworth Adhesive (Germantown, WI). Lactate oxidase (80 U) was purchased from Toyobo (Osaka, Japan). Acetic acid was purchased from Fisher Science (Hampton, NH). The gold electrode (2 mm dia.), Ag/AgCl electrode, and platinum electrode were all purchased from CH instruments (Austin, TX) for standard electrochemical testing. Polyimide was purchased from HD Microsystems (Parlin, NJ), poly(methylmethacrylate) (PMMA) 495A5 was purchased from Microchem (Westborough, MA). Nitrogen and oxygen gas tanks were purchased from Airgas (Radnor, PA). Water-soluble tape (3 M) was purchased from Digikey (Thief River Falls, MN). Anisotropic conductive film was purchased from Elform (Fallon, NV). Isopropyl alcohol and acetone were purchased from BDH Chemicals (Radnor, PA). Tecophilic (HP-93A-100) and Tecoflex (SG-80A) were received from Lubrizol LifeSciences (Cleveland, OH) as a gift.

2.2. Structure design and mechanical testing of skin-inspired hierarchical lattice material

To determine the ideal deterministic architecture, size iterations of the bio-inspired hierarchical lattice structure were established in relation to the circular electrode interconnects. The mechanical properties of the proposed structures with varying unit lengths were examined through tensile testing. An INSTRON tensiometer with a 500 N capacity load cell at 3 mm/min was used. Polyimide film (thickness = 25 μm) cutouts with deterministically patterned lattice structures were fabricated by laser engraving (Universal Laser System, VLS3.5) with 1000 ppi, 40% power, and 100% speed, to etch an electrode radius of 1 cm and varying serpentine unit lengths: small (1.5 cm), medium (2.25 cm), and large (3.0 cm) (Fig. 1A). The mean and standard deviation for ultimate tensile strength (UTS) and Young's modulus were calculated, along with the yield strength elongation and total elongation.

Final microfabricated devices were transfer printed onto commercial wound dressings that are textile-silicone (ScarAway – Silicone Scar Sheets) and polymeric (Walgreens – Silicone Scar Sheets). Tensile testing of the device on the wound dressing substrate was then evaluated. The Young's modulus, UTS, yield strength elongation, and total elongation were calculated.

2.3. Microfabrication of the flexible and stretchable device

The microfabrication of the flexible and stretchable gold electrodes follows previously published methods (Lee et al., 2017b) and described in the details in the Supplementary information (SI Fig. 1). Computer-assisted designs (CAD) were developed and used for microfabrication of the device (Fig. 1A). Fabrication consisted of a silicon wafer that was cleaned, spin coated, and cured with PMMA and PI (~1.2 μm), respectfully. Subsequently, chrome (5 nm) and gold (200 nm) was deposited and patterning was executed through conventional photolithography techniques, yielding a geometrically patterned gold design. A final PI layer was spin coated, encapsulating the gold layer. Reactive ion etching (RIE) (20 ss cm of O_2, 300 mTorr, 100 W for 30 min) defined lattice structures and an open area of the gold electrode using a metal mask that was photolithographically defined Cr (50 nm). After defining the sensing interface and dissolving the sacrificial layer of PMMA by immersing the device in acetone for 1 h, the sensor was transfer printed onto water-soluble tape (3 M). Following this, Ti (5 nm)/and SiO_2 (50 nm) were deposited on the back of the sensor and the patterned sensor was transferred onto a silicon bandage, which serves as a soft substrate. The next step in developing the electrochemical sensors involved dissolving the water-soluble tape and drying the device in ambient conditions. An anisotropic conductive film (ACF) attached to the bonding pad connected the device to the potentiostat for further testing.

2.4. Fabrication of lactate sensor

The SWCNT solutions were prepared with 2% acetic acid (0.2 mg/mL, magnetic stirring for 30 min at 20 °C) and combined with chitosan to form a 1% chitosan mixture (sonic agitation for 20 min, magnetic stirring for 2 h). Prussian blue was formed using 100 mM KCl, 2.5 mM $K_3Fe(CN)6$, 2.5 mM $FeCl_3$, and 100 mM HCl. A Prussian blue mediator layer was electrochemically deposited on the electrode surfaces (Fig. 3A) through cyclic voltammetry (−0.5 to 0.6 V vs. Ag/AgCl (sat' KCl), 0.05 V/s scan rate for 10 cycles). After the deposition and rinsing the electrodes with DI water, 66 μL of 1% chitosan/SWCNT/acetic acid solution was drop casted onto the gold electrode surface and allowed to dry for 20 min. Proceeding, 44 μL of lactate oxidase solution (50 mg/mL in phosphate buffered saline (PBS, pH 7.4)) was drop casted on the surface and allowed to dry for 20 min. Finally, another 66 μL of 1% chitosan/SWCNT/acetic acid solution was drop casted on the electrode surface. The substrate was stored for 1 day at 4 °C.

2.5. Fabrication of oxygen sensor

The gold electrode was first exposed to ultraviolet (UV) light (Compact UV-Ozone Cleaner, EQ-PCE-44-LD) for 2 min to increase adhesion among the selective membrane layers. Then, Nafion was drop casted onto the gold electrode while conducting 3 iterations of 5 μL of Nafion to spread out evenly on the gold surface followed by drying for 45 min at room temperature. The selective diffusion membrane was formed by casting 30 μL of 30–40 wt% PDMS concentration diluted with toluene. The PDMS mixture was then cured in an oven at 60 °C for 1 h.

2.6. Evaluation of electrochemical sensor performance

We used chronoamperometry produced by a CH Instruments 1080 Potentiostat (Austin, TX) to evaluate the sensitivity, dynamic range, and response time of the fabricated electrochemical sensors. All electrochemical analysis was conducted with three-electrode systems in 10 mM PBS (pH 7.4) at room temperature. The Ag/AgCl (sat' KCl) served as a reference electrode while platinum wire electrode was used as a counter electrode. The electrochemical response was monitored by injecting lactate stock solution or by modulating the gas concentration by changing the ratio of oxygen and nitrogen gas with the proportioner under flow of 120 psig. The dissolved oxygen concentration in the PBS was determined using standard HI 2040 multiparameter DO meter (Hanna Instrument; Woonsocket, RI). The applied electrode potentials were +0.6 vs. Ag/AgCl and −0.4 V vs. Ag/AgCl for lactate and oxygen sensors, respectively.

3. Results and discussion

3.1. Mechanical quantification of deterministic, triangular lattice structures

Table 1 and Fig. 1A–E present the mechanical properties distinct to each variation in serpentine unit length. Under weak strains the triangular structures expanded and exhibited minimal resistance, with characteristic homologues to elastin fibers (Holzapfel, 2001). In contrast, stronger strains caused the structures to exhibit a rigid characteristic — increased modulus (Jang et al., 2015). Additionally, in comparison to the skin, the geometries were capable of adjusting to similar, non-linear stress, homologous to skin (Fig. 1C–F) (Holzapfel, 2001). The small design presented the smallest Young's modulus, 3.85 ± 1.62 MPa, while medium design as the largest, 6.92 ± 2.39 MPa, and large design as intermediate, 5.16 ± 2.78 MPa. All designs exhibited a modulus within the range of skin's (5 kPa to 140 MPa) (Kwon et al., 2018). Further, additional design considerations included electrode density and yield strength elongation %. Electrodes with large voids between each iteration present a decrease in sensor spatial resolution in electrochemical detection because of the reduction in surface area, negatively impacting sensor performance. Therefore, the small and medium patterns were regarded as superior design geometries, with the medium design exhibiting a desirable yield strength elongation 29.62 ± 3.59% to allow for the device to cyclically stretch and not plastically deform, which is similar to that of skin, 30% (Dickey, 2016). The actual microfabricated device was designed and fabricated with the same ratio as the medium design (2.25) in relation of lattice size to electrode diameter encapsulation. Therefore, the final design yielded a lattice size of 1.575 mm with a unit electrode encapsulation size of 0.7 mm (Fig. 2B).

Table 2 and Fig. 1F–G present the mechanical properties of the microfabricated device, transfer printed onto a polymeric and textile-silicone based wound dressing. Testing revealed that the overall device exhibited desired characteristics on the dressings; however, the textile-silicone dressing was capable of an increased modulus 6.09 MPa and yield strength elongation 47.26% in comparison to the polymeric dressing's modulus, 4.12 MPa and yield strength elongation, 25.72% (Fig. 1F). The device was capable of exhibiting a desirable modulus with the textile-silicone and polymeric dressing. However, the textile-silicon dressing exhibited increased robustness, as the yield strength elongation was higher, therefore, the device was capable of cyclically stretching in response to greater strains without plastic deforming.

Table 1
Mechanical properties of deterministic, triangular lattice structure designs.

Sample	Ultimate tensile strength (MPa)	Young's Modulus (MPa)	Yield strength elongation (%)	Elongation (%)
PI film	151.02 ± 2.10	2242.09 ± 63.36	1.80 ± 0.31	26.87 ± 7.57
Small	0.37 ± 0.08	3.85 ± 1.62	21.65 ± 1.73	62.92 ± 14.23
Medium	0.52 ± 0.04	6.92 ± 2.39	29.62 ± 3.59	106.52 ± 3.88
Large	0.55 ± 0.15	5.16 ± 2.78	36.63 ± 3.06	161.64 ± 40.96

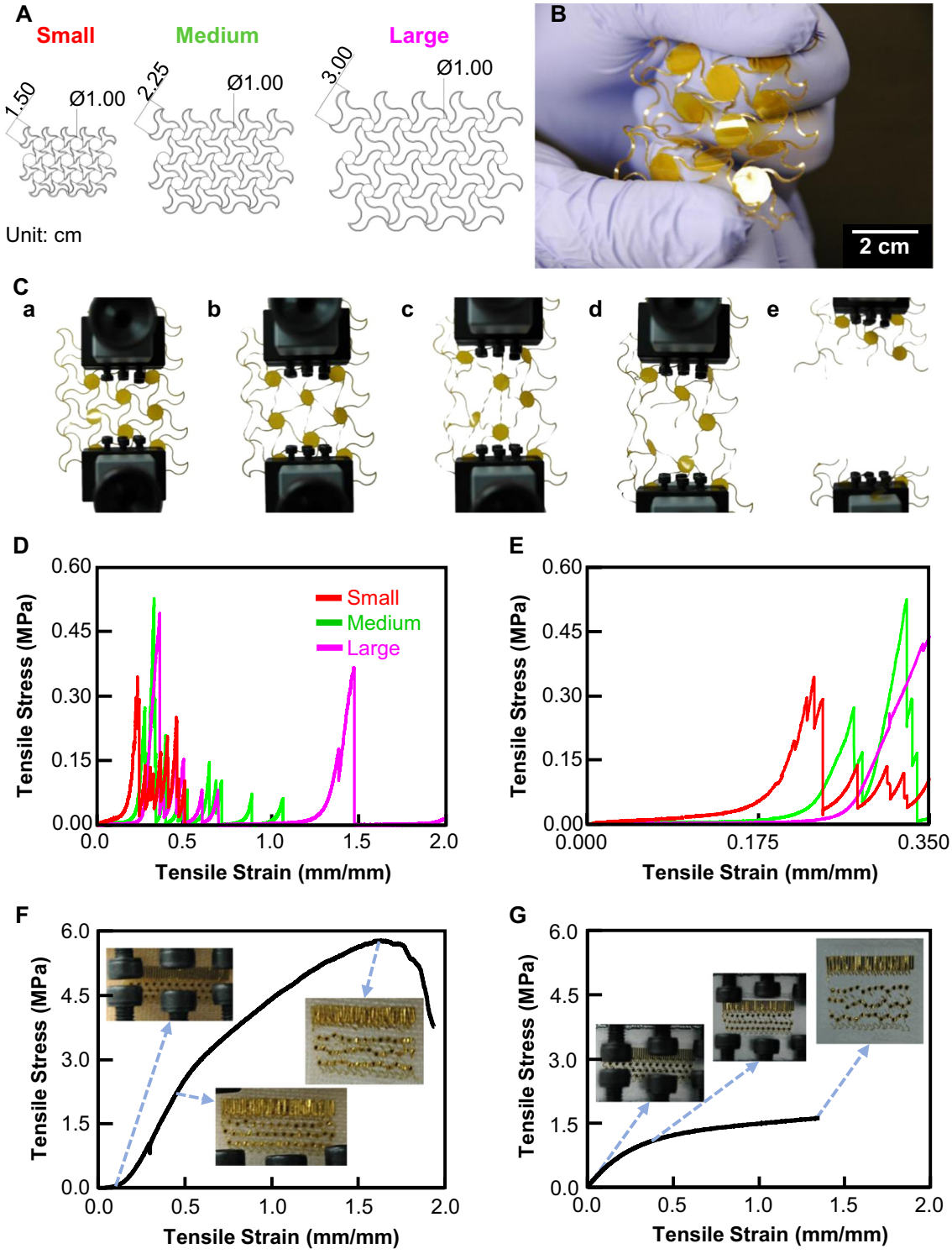

Fig. 1. Device Mechanical Testing. (A) Schematic device design using polyimide cutouts for mechanical testing purposes. Designs were cut using laser engraving with 1000 ppi, 40% power, and 100% speed. Small device represents 1.5 cm (red), medium represents 2.25 cm (green), and large device (magenta) represents 3.0 cm triangular repeating unit lengths. (B) Image of small design. (C) Tensiometer testing of medium sample: a) toe region, b) elastic region, c) ultimate tensile strength, d) breaking strength, e) failure. (D-G) (n = 3) Tensile stress and strain measurements of sets closest to each average design, using 3 mm/min strain rate. (D) Complete data for each sample test: small, medium, and large. (E) Data from beginning to first break. (F-G) (n = 1) Tensile testing of microfabricated device on commercial wound dressings and corresponding images of the device at: start, yield strength, and failure. (F) Textile-silicone wound dressing (ScarAway – Silicone Scar Sheets). (G) Polymeric wound dressing (Walgreens – Silicone Scar Sheets).

3.2. Skin-inspired gold electrodes for electrochemical biosensors

As the medium overlapping electrodes (i.e., nodes) to triangular lattice structure exhibit suitable mechanical properties for skin-mountable electronics with minimal reduction in spatial resolution, this design was chosen as the model electrode system. The bare gold surface exposed at each node (circular electrode) allows modifying biorecognitive membranes while insulating other parts with polyimide (PI).

Table 2
Mechanical properties of microfabricated sensor laminated on commercial wound dressings.

Dressing	Ultimate tensile strength (MPa)	Young's Modulus (MPa)	Yield strength elongation (%)	Elongation (%)
Polymeric	1.57	4.12	25.72	136.03
Textile-silicone	5.15	6.09	47.26	193.85

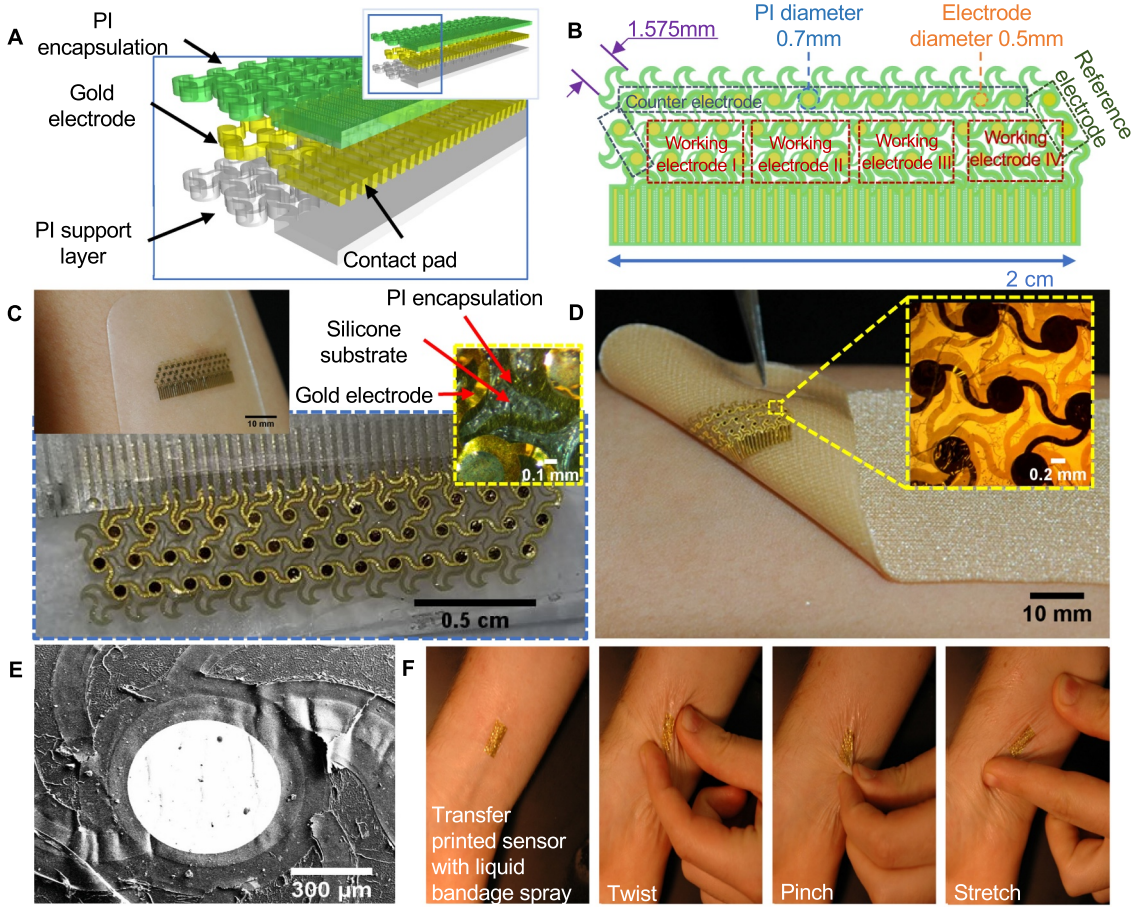

Fig. 2. Skin-inspired gold electrodes (A) Schematic diagram of the flexible device. (B) Schematic diagram with dimensions. (C) Image of the sensor on polymeric wound dressing (Walgreens – Silicone Scar Sheets). (D) Image of the sensor on a textile-silicon bandage (ScarAway – Silicone Scar Sheets). (E) SEM image of electrode. (F) Pictures of device under mechanical distortion (twisting, pinching, and stretching).

The wires are interconnected with a lithographically defined lattice horseshoe structures meta-design that allows biaxial stretchability and bonding pads connect the device to the potentiostat for further electrochemical analysis. Fig. 2 shows the schematic diagram of the electrode design and representative thin, skin-inspired gold electrodes on substrates of silicone polymers, commercially available wound dressings, or directly on the skin. The array of gold electrodes (dia. 500 μm) with the total thickness of ~3.3 μm (5 nm Cr/200 nm Au encapsulated with 1.5 μm PI on each side) provides the sensing interface as a bundle. In this particular design, the six electrodes work as one electrochemical sensor. The structure governs free mass transfer across the soft elastomeric substrates and thus prevents accumulation on the interface between the device and biology.

3.3. Lactate sensor on triangular network architectures for real-time analysis

Fig. 3 summarizes key metrics that validate and characterize lactate sensing performance. The electrochemical deposition of Prussian blue was achieved through cyclic voltammetry with a scan rate of 50 mV/s for 10 cycles from −0.6–0.5 V vs. Ag/AgCl. (Fig. 3B). The positive voltage from the first sweep established a thermodynamically favorable form for Prussian blue to exist in ion form. The Prussian blue layer contributed to increasing lactate sensor sensitivity by two orders of magnitude (1.973 μA/mM for Prussian blue compared with 0.053 μA/mM without Prussian blue) (Fig. 3C). Response time ($t_{90\%}$) and dynamic range were similar; 28.5 s with 0.1–0.5 mM and 28.3 s with 0.1–0.4 mM for the sensor with and without Prussian blue layer, respectively. These results confirm using Prussian blue to improve lactate detection. In addition, the presence of SWCNTs reduced the sensor's response time by half while exhibiting 47.1 s and 95.5 s of $t_{90\%}$ for with and without SWCNTs in the chitosan matrix, respectively (Fig. 3D). However, the sensitivity slightly decreased from 1.374 μA/mM to 0.892 μA/mM by introducing SWCNTs. This results from reactions caused by hydrogen peroxide competing with the Prussian blue layer for transduction and electrode detection (Tkac and Ruzgas, 2006). The addition of chitosan embedded in acetic acid provides a viscous film that immobilizes the lactate oxidase enzyme against the electrode's surface while maintaining catalytic performance. Along with cyclic voltammetry, scanning electron microscopy (SEM), Fourier-transformed infrared spectroscopy (FTIR), and electrochemical impedance spectroscopy (EIS) have reported in comparable lactate sensor research (Cui et al., 2007; Kaushik

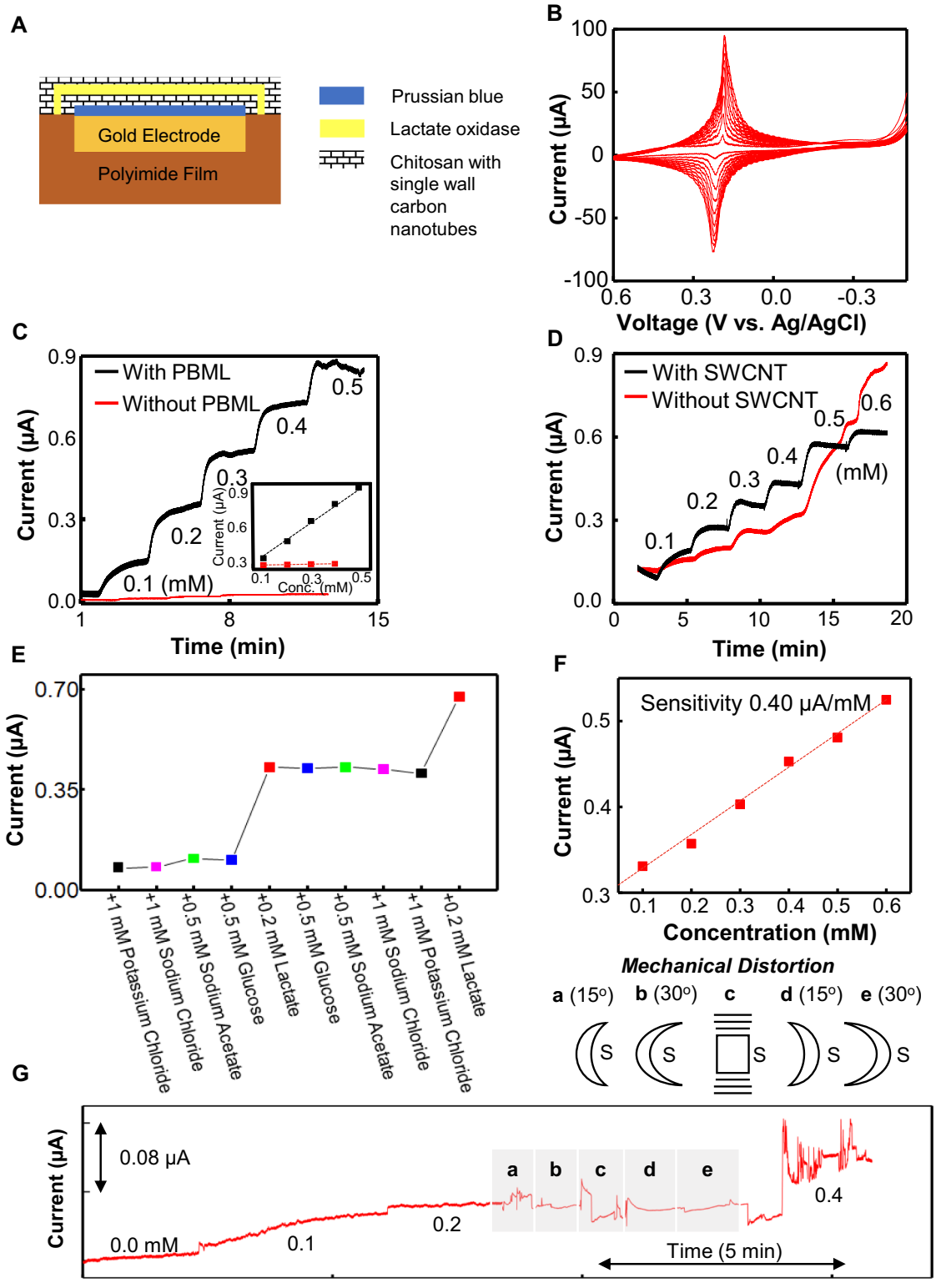

Fig. 3. Lactate Sensor Characteristics. (A) Schematic of electrode. (B) Cyclic voltammogram of the electrode. (C) Effects of Prussian blue on electrochemical lactate detection, with 25 cyclic voltammetry cycles in Prussian blue mediator layer (black) compared to no cyclic voltammetry cycles (red). (D) Impact of single-walled carbon nanotubes (SWCNT) on sensor performance, with SWCNTs (black) versus no SWCNTs (red) in chitosan layer. (E) Specificity of lactate concentration. (F) The calibration curve of current vs. concentration. (G) Electrochemical results when undergoing mechanical stress. Testing done with sensor attached to PDMS and submerged in PBS. (a) 15° concave, (b) 30° concave, (c) tensile stretching, (d) 15° convex, and (e) 30° convex configuration. (For interpretation of the references to color in this figure legend, the reader is referred to the web version of this article.)

et al., 2010). Of note, although the sensitivity is lower than without carbon nanotubes, the improvement brought forth in response time and linearity transcends the variation in sensitivity.

The lactate sensor was further characterized in a PBS solution with various analytes to observe the selectivity of the sensor for lactate (Fig. 3E). In relation to other biological biomarkers (e.g., sodium, potassium, chlorine, glucose, etc.), the sensor can differentiate and express high sensitivity for lactate ($p < 0.05$). The sensor was also selective to lactate compared to molecules of similar shape and composition (e.g., acetate and ascorbates). Lactate change was detectable even with high concentrations of interfering analytes in solution, exhibited by a similar linear response. Further evidence is determined by calculating selectivity coefficients for the different biomarkers given from the following equation:

$$\log(K_{lac,\ j}^{amp}) = \log\left(\frac{\Delta I_j/c_j}{\Delta I_{lac}/c_{lac}}\right) \quad (1)$$

where I is current, c is concentration, and j represents a variant of the other biomarkers tested against. Selectivity coefficients were determined as −2.89, −1.45, −2.05, and −2.16 for sodium chloride,

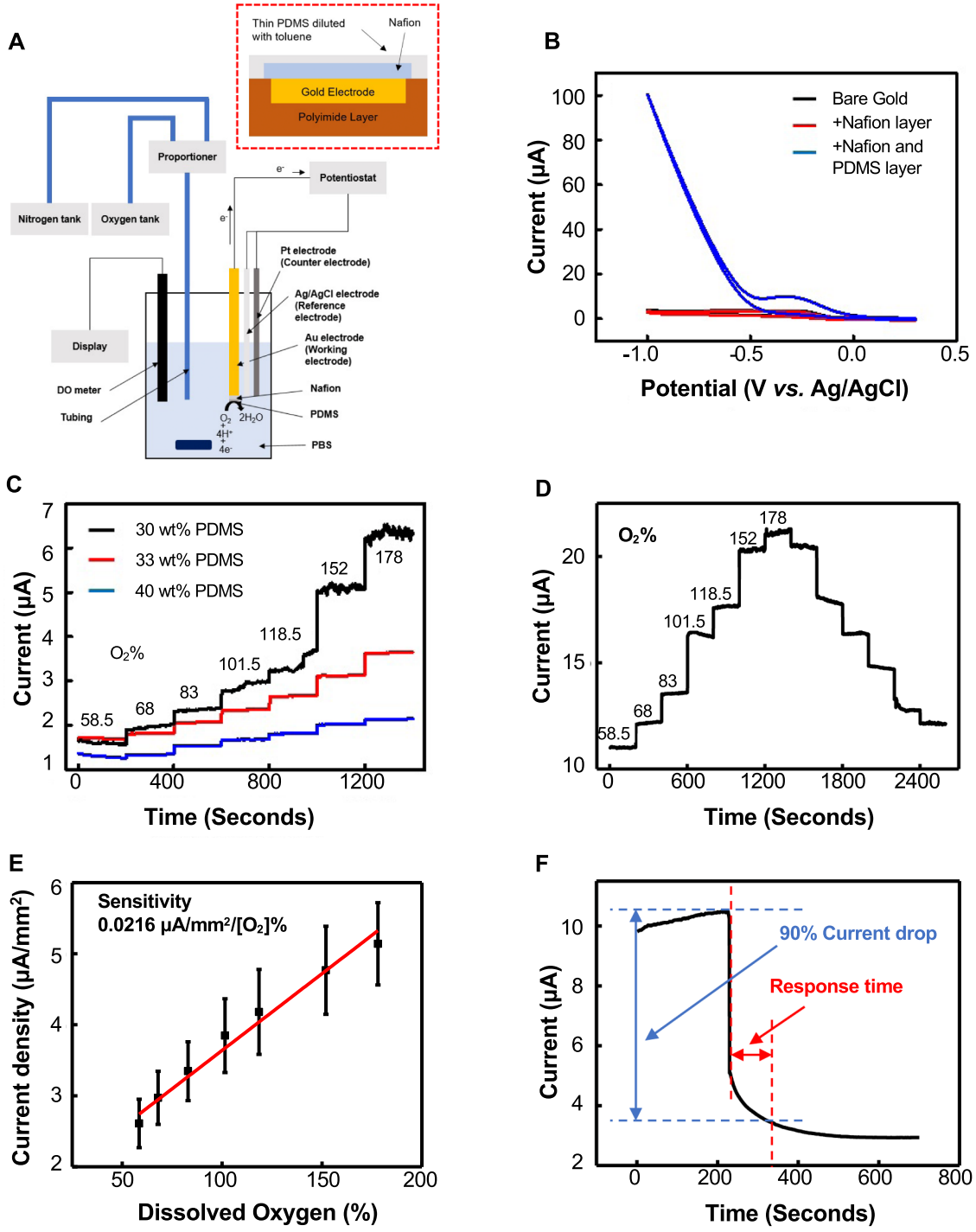

Fig. 4. Oxygen Sensor Characteristics. (A) Experimental set-up for the Clark-type oxygen sensor. (B) Cyclic voltammogram for the evaluation of the effect Nafion and PDMS membranes have on the gold electrode. (C) Amperometric i–t curves of the sensor with various PDMS wt%. (D) Amperometric i–t curves of the sensor. (E) The calibration curve of current density vs. dissolved oxygen. (F) Sensor response time, from oxygen saturated state to oxygen depleted state.

sodium acetate, potassium chloride, and glucose, respectively, comparable to appropriate selectivity values from successful lactate sensors (Ricci and Palleschi, 2005). Changing temperature characterizations were also determined and presented in the Supplemental information (SI Fig. 2).

Fig. 3F shows the sensitivity curve demonstrated with microfabricated enzymatic lactate sensing. With a sensitivity of 0.395 μA/mM, values are comparable to the previously analyzed lactate sensors as they are within the same order for current amplitude, response time, and dynamic range. Lactate sensing under mechanical distortions was also studied. The skin-like lactate sensor underwent changes in structural configurations while submerged in a 0.2 mM lactate solution (Fig. 3G). The graph displays slight current changes because of mechanical distortions. However, changes did not significantly deviate from current values without mechanical stresses applied at the same lactate concentration ($p > 0.05$). Small current variations may be from the varying microscopic area of exposed gold that interacts with the solution as it undergoes mechanical stress and thus the continuously changes resistance from changing conductive surface area directly led to fluctuations in the recorded current. The device also responded to lactate following mechanical distortions with current change consistent with previously non-deformed models, confirming lactate sensor durability and robustness under biomaterial stresses.

3.4. Oxygen Sensor on triangular network architectures for real-time analysis

The electrochemical oxygen sensor was fabricated as shown in Fig. 4. Performance of the Clark-type oxygen sensor was studied based on the effect of Nafion and diluted PDMS. The electrochemical reaction was characterized by cyclic voltammetry for bare gold, electrodes coated with the Nafion layer, and electrodes coated with Nafion and PDMS layer (Fig. 4B). Cyclic voltammogram shows amplification of the reduction current at around −0.25 V vs. Ag/AgCl with a single bias point for oxygen reduction without a competing reaction. While the bare gold and Nafion layer coated electrodes exhibited small peaks at −0.3 V and −0.5 V vs. Ag/AgCl, the oxygen sensor with the PDMS and Nafion layer amplified the potential at −0.4 V with a significant increase in current response. Of note, the PDMS layer serves as an oxygen selective membrane because of the hydrophobic character and allows the superior electrochemical response to dissolved oxygen.

The sensitivity of the oxygen sensor was quantified in relation to varying PDMS concentrations (Fig. 4C). The oxygen sensor with a 30 wt % PDMS membrane exhibited the highest sensitivity 29 nA/[O_2]%, while the sensitivity decreased with the increasing wt% layers to 16 nA/[O_2]% and 8.7 nA/[O_2]% for 33% and 40% PDMS, respectively. As the PDMS was diluted with the addition of toluene, sensitivity increased while the stability of the signal decreased due to changes of membrane thickness. The thickness of PDMS films were 4.87, 6.88, and 11.55 μm for 30, 33, and 40 wt% PDMS membrane, respectively. The sensor was capable of detecting increases and decreases in the concentration of dissolved oxygen. Finally, the soft, skin-like oxygen sensor was capable of exhibiting a sensitivity of 21.6 nA/[O_2]% (Fig. 4E) and exhibited 69 s of the response time ($t_{90\%}$). (Fig. 4F). The dynamic range was determined from 58.5 to 178 [O_2]%. The normal oxygen concentration in human blood ranges from 1.60 to 4.16 mg/L (10.5–27.7 [O_2]%), while air saturated biological fluids contain oxygen concentration near 8 mg/L (53.3 [O_2]%) (Pita et al., 2013). Further studies are underway to optimize the sensor performance for biomedical applications.

4. Conclusion

The soft, lattice sensors were successfully demonstrated in engineering, development, and analytical assessments of the deterministically patterned electrochemical biosensors capable of real-time lactate and oxygen monitoring. The deterministic structure allowed for mechanically-compliant and durable sensors capable of maintaining high-performance sensing while deforming to applied strains similar to skin. The investigations of the skin-like sensors allow for the determination of lactate from 0.05 to 0.85 mM and oxygen from 58.5 to 178 [O_2]%. Conducting results for lactate and oxygen monitoring on a flexible device as a feasible method can allow for future research in more specific clinical applications such as sweat, chronic wound exudate, or other on-skin biofluid monitoring. The sensor performance and feasibility could be further improved through implementations of a hybrid sensor (e.g., glucose, sodium, and potassium) and membrane modification that necessary for clinical applications. The studies of in vivo sensor performance are underway.

Acknowledgments

We acknowledge the support of Small Scale Systems Integration and Packaging (S3IP) Center of Excellence and Integrated Electronics Engineering Center (IEEC) at SUNY Binghamton. We also acknowledge the supports from Binghamton University's Health Sciences Transdisciplinary Area of Excellence and Start-up funds.

Credit author statement

BA and MB were the equality contributed first authors writing the manuscript. BA, MB, and YP performed the experiments and analyzed the experimental data. SK conduct the mechanical testing. AK designed the experiment, supervised this work and provided guidance and assistance in drafting the manuscript as a corresponding author.

Declaration of interests

None.

Appendix A. Supporting information

Supplementary data associated with this article can be found in the online version at doi:10.1016/j.bios.2019.02.041.

References

Bandodkar, A.J., Hung, V.W., Jia, W., Valdes-Ramirez, G., Windmiller, J.R., Martinez, A.G., Ramirez, J., Chan, G., Kerman, K., Wang, J., 2013. Tattoo-based potentiometric ion-selective sensors for epidermal pH monitoring. Analyst 138 (1), 123–128.

Bandodkar, A.J., Jia, W., Yardımcı, C., Wang, X., Ramirez, J., Wang, J., 2015. Tattoo-based noninvasive glucose monitoring: a proof-of-concept study. Anal. Chem. 87 (1), 394–398.

Brown, M.S., Ashley, B., Koh, A., 2018. Wearable technology for chronic wound monitoring: current dressings, advancements, and future prospects. Front. Bioeng. Biotechnol. 6, 47.

Cui, X., Li, C.M., Zang, J., Yu, S., 2007. Highly sensitive lactate biosensor by engineering chitosan/PVI-Os/CNT/LOD network nanocomposite. Biosens. Bioelectron. 22 (12), 3288–3292.

Dagdeviren, C., Su, Y., Joe, P., Yona, R., Liu, Y., Kim, Y.-S., Huang, Y., Damadoran, A.R., Xia, J., Martin, L.W., Huang, Y., Rogers, J.A., 2014. Conformable amplified lead zirconate titanate sensors with enhanced piezoelectric response for cutaneous pressure monitoring. Nat. Commun. 5, 4496.

Dickey, M.D., 2016. Liquid metals for soft and stretchable electronics. In: Rogers, J.A., Ghaffari, R., Kim, D.-H. (Eds.), Stretchable Bioelectronics for Medical Devices and Systems. Springer International Publishing, Switzerland, pp. 3–30.

Fan, J.A., Yeo, W.-H., Su, Y., Hattori, Y., Lee, W., Jung, S.-Y., Zhang, Y., Liu, Z., Cheng, H., Falgout, L., Bajema, M., Coleman, T., Gregoire, D., Larsen, R.J., Huang, Y., Rogers, J.A., 2014. Fractal design concepts for stretchable electronics. Nat. Commun. 5, 3266.

Flynn, C., Taberner, A., Nielsen, P., 2011. Mechanical characterisation of in vivo human skin using a 3D force-sensitive micro-robot and finite element analysis. Biomech. Model. Mechanobiol. 10 (1), 27–38.

Gao, W., Emaminejad, S., Nyein, H.Y.Y., Challa, S., Chen, K., Peck, A., Fahad, H.M., Ota, H., Shiraki, H., Kiriya, D., Lien, D.-H., Brooks, G.A., Davis, R.W., Javey, A., 2016. Fully integrated wearable sensor arrays for multiplexed in situ perspiration analysis. Nature 529, 509.

Gong, S., Schwalb, W., Wang, Y., Chen, Y., Tang, Y., Si, J., Shirinzadeh, B., Cheng, W., 2014. A wearable and highly sensitive pressure sensor with ultrathin gold nanowires. Nat. Commun. 5, 3132.

Ha, M., Lim, S., Park, J., Um, D.-S., Lee, Y., Ko, H., 2015. Bioinspired interlocked and

hierarchical design of ZnO nanowire arrays for static and dynamic pressure-sensitive electronic skins. Adv. Funct. Mater. 25 (19), 2841–2849.
Hattori, Y., Falgout, L., Lee, W., Jung, S.-Y., Poon, E., Lee, J.W., Na, I., Geisler, A., Sadhwani, D., Zhang, Y., Su, Y., Wang, X., Liu, Z., Xia, J., Cheng, H., Webb, R.C., Bonifas, A.P., Won, P., Jeong, J.-W., Jang, K.-I., Song, Y.M., Nardone, B., Nodzenski, M., Fan, J.A., Huang, Y., West, D.P., Paller, A.S., Alam, M., Yeo, W.-H., Rogers, J.A., 2014. Multifunctional skin-like electronics for quantitative, clinical monitoring of cutaneous wound healing. Adv. Healthc. Mater. 3 (10), 1597–1607.
Heikenfeld, J., Jajack, A., Rogers, J., Gutruf, P., Tian, L., Pan, T., Li, R., Khine, M., Kim, J., Wang, J., Kim, J., 2018. Wearable sensors: modalities, challenges, and prospects. Lab Chip 18 (2), 217–248.
Holzapfel, Gerhard A., 2001. Biomechanics of soft tissue. In: LeMaitre, J. (Ed.), Handbook of Materials Behavior Models. Academic Press, Graz, Austria, pp. 1057–1071.
Hua, Q., Sun, J., Liu, H., Bao, R., Yu, R., Zhai, J., Pan, C., Wang, Z.L., 2018. Skin-inspired highly stretchable and conformable matrix networks for multifunctional sensing. Nat. Commun. 9 (1), 244.
Hwang, S.W., Tao, H., Kim, D.H., Cheng, H., Song, J.K., Rill, E., Brenckle, M.A., Panilaitis, B., Won, S.M., Kim, Y.S., Song, Y.M., Yu, K.J., Ameen, A., Li, R., Su, Y., Yang, M., Kaplan, D.L., Zakin, M.R., Slepian, M.J., Huang, Y., Omenetto, F.G., Rogers, J.A., 2012. A physically transient form of silicon electronics. Science 337 (6102), 1640–1644 (New York, N.Y.).
Imani, S., Bandodkar, A.J., Mohan, A.V., Kumar, R., Yu, S., Wang, J., Mercier, P.P., 2016. A wearable chemical–electrophysiological hybrid biosensing system for real-time health and fitness monitoring. Nat. Commun. 7, 11650.
Jang, K.-I., Han, S.Y., Xu, S., Mathewson, K.E., Zhang, Y., Jeong, J.-W., Kim, G.-T., Webb, R.C., Lee, J.W., Dawidczyk, T.J., 2014. Rugged and breathable forms of stretchable electronics with adherent composite substrates for transcutaneous monitoring. Nat. Commun. 5, 4779.
Jang, K.-I., Chung, H.U., Xu, S., Lee, C.H., Luan, H., Jeong, J., Cheng, H., Kim, G.-T., Han, S.Y., Lee, J.W., 2015. Soft network composite materials with deterministic and bio-inspired designs. Nat. Commun. 6, 6566.
Jeong, J.-W., Kim, M.K., Cheng, H., Yeo, W.-H., Huang, X., Liu, Y., Zhang, Y., Huang, Y., Rogers, J.A., 2014. Capacitive epidermal electronics for electrically safe, long-term electrophysiological measurements. Adv. Healthc. Mater. 3 (5), 642–648.
Jiang, Y., Wang, Q., 2016. Highly-stretchable 3D-architected mechanical metamaterials. Sci. Rep. 6, 34147.
Kang, S.K., Murphy, R.K., Hwang, S.W., Lee, S.M., Harburg, D.V., Krueger, N.A., Shin, J., Gamble, P., Cheng, H., Yu, S., Liu, Z., McCall, J.G., Stephen, M., Ying, H., Kim, J., Park, G., Webb, R.C., Lee, C.H., Chung, S., Wie, D.S., Gujar, A.D., Vemulapalli, B., Kim, A.H., Lee, K.M., Cheng, J., Huang, Y., Lee, S.H., Braun, P.V., Ray, W.Z., Rogers, J.A., 2016. Bioresorbable silicon electronic sensors for the brain. Nature 530 (7588), 71–76.
Kaushik, A., Solanki, P.R., Pandey, M.K., Kaneto, K., Ahmad, S., Malhotra, B.D., 2010. Carbon nanotubes — chitosan nanobiocomposite for immunosensor. Thin Solid Films 519 (3), 1160–1166.
Kim, D.-H., Rogers, J.A., 2008. Stretchable electronics: materials strategies and devices. Adv. Mater. 20 (24), 4887–4892.
Kim, D.-H., Lu, N., Huang, Y., Rogers, J.A., 2012. Materials for stretchable electronics in bioinspired and biointegrated devices. MRS Bull. 37 (3), 226–235.
Kim, J., Salvatore, G.A., Araki, H., Chiarelli, A.M., Xie, Z., Banks, A., Sheng, X., Liu, Y., Lee, J.W., Jang, K.-I., Heo, S.Y., Cho, K., Luo, H., Zimmerman, B., Kim, J., Yan, L., Feng, X., Xu, S., Fabiani, M., Gratton, G., Huang, Y., Paik, U., Rogers, J.A., 2016. Battery-free, stretchable optoelectronic systems for wireless optical characterization of the skin. Sci. Adv. 2 (8).
Koh, A., Kang, D., Xue, Y., Lee, S., Pielak, R.M., Kim, J., Hwang, T., Min, S., Banks, A., Bastien, P., Manco, M.C., Wang, L., Ammann, K.R., Jang, K.-I., Won, P., Han, S., Ghaffari, R., Paik, U., Slepian, M.J., Balooch, G., Huang, Y., Rogers, J.A., 2016. A Soft, Wearable microfluidic device for the capture, storage, and colorimetric sensing of sweat. Sci. Transl. Med. 8 (366) (366ra165-366ra165).
Krishnan, S., Shi, Y., Webb, R.C., Ma, Y., Bastien, P., Crawford, K.E., Wang, A., Feng, X., Manco, M., Kurniawan, J., Tir, E., Huang, Y., Balooch, G., Pielak, R.M., Rogers, J.A., 2017. Multimodal epidermal devices for hydration monitoring. Microsyst. Amp Nanoeng. 3, 17014.
Kwon, S.H., Padmanabhan, J., Gurtner, G.C., 2018. Chapter 14 - Mechanobiology of skin diseases and wound healing. In: Verbruggen, S.W. (Ed.), Mechanobiology in Health and Disease. Academic Press, pp. 415–448. https://doi.org/10.1016/B978-0-12-812952-4.00014-3. ISBN 9780128129524. http://www.sciencedirect.com/science/article/pii/B9780128129524000143.
Lee, H., Choi, T.K., Lee, Y.B., Cho, H.R., Ghaffari, R., Wang, L., Choi, H.J., Chung, T.D., Lu, N., Hyeon, T., Choi, S.H., Kim, D.-H., 2016. A graphene-based electrochemical device with thermoresponsive microneedles for diabetes monitoring and therapy. Nat. Nanotechnol. 11, 566.
Lee, H., Song, C., Hong, Y.S., Kim, M.S., Cho, H.R., Kang, T., Shin, K., Choi, S.H., Hyeon, T., Kim, D.-H., 2017a. Wearable/disposable sweat-based glucose monitoring device with multistage transdermal drug delivery module. Sci. Adv. 3 (3).
Lee, Y.K., Jang, K.-I., Ma, Y., Koh, A., Chen, H., Jung, H.N., Kim, Y., Kwak, J.W., Wang, L., Xue, Y., Yang, Y., Tian, W., Jiang, Y., Zhang, Y., Feng, X., Huang, Y., Rogers, J.A., 2017b. Chemical sensing systems that utilize soft electronics on thin elastomeric substrates with open cellular designs. Adv. Funct. Mater. 27 (9), 1605476.
Liu, L., Yu, Y., Yan, C., Li, K., Zheng, Z., 2015. Wearable energy-dense and power-dense supercapacitor yarns enabled by scalable graphene–metallic textile composite electrodes. Nat. Commun. 6, 7260.
Liu, Y., Norton, J.J., Qazi, R., Zou, Z., Ammann, K.R., Liu, H., Yan, L., Tran, P.L., Jang, K.I., Lee, J.W., Zhang, D., Kilian, K.A., Jung, S.H., Bretl, T., Xiao, J., Slepian, M.J., Huang, Y., Jeong, J.W., Rogers, J.A., 2016. Epidermal mechano-acoustic sensing electronics for cardiovascular diagnostics and human-machine interfaces. Sci. Adv. 2 (11), e1601185.
Liu, Y., Pharr, M., Salvatore, G.A., 2017. Lab-on-skin: a review of flexible and stretchable electronics for wearable health monitoring. ACS Nano 11 (10), 9614–9635.
Liu, Z., Yu, M., Lv, J., Li, Y., Yu, Z., 2014. Dispersed, porous nanoislands landing on stretchable nanocrack gold films: maintenance of stretchability and controllable impedance. ACS Appl. Mater. Interfaces 6 (16), 13487–13495.
Lochner, C.M., Khan, Y., Pierre, A., Arias, A.C., 2014. All-organic optoelectronic sensor for pulse oximetry. Nat. Commun. 5, 5745.
Luo, J., Dziubla, T., Eitel, R., 2017. A low temperature co-fired ceramic based microfluidic clark-type oxygen sensor for real-time oxygen sensing. Sens. Actuators B: Chem. 240, 392–397.
Ma, Q., Cheng, H., Jang, K.-I., Luan, H., Hwang, K.-C., Rogers, J.A., Huang, Y., Zhang, Y., 2016. A nonlinear mechanics model of bio-inspired hierarchical lattice materials consisting of horseshoe microstructures. J. Mech. Phys. Solids 90, 179–202.
Matsuhisa, N., Kaltenbrunner, M., Yokota, T., Jinno, H., Kuribara, K., Sekitani, T., Someya, T., 2015. Printable elastic conductors with a high conductivity for electronic textile applications. Nat. Commun. 6, 7461.
Nie, Z., Deiss, F., Liu, X., Akbulut, O., Whitesides, G.M., 2010a. Integration of paper-based microfluidic devices with commercial electrochemical readers. Lab chip 10 (22), 3163–3169.
Nie, Z., Nijhuis, C.A., Gong, J., Chen, X., Kumachev, A., Martinez, A.W., Narovlyansky, M., Whitesides, G.M., 2010b. Electrochemical sensing in paper-based microfluidic devices. Lab chip 10 (4), 477–483.
Pita, M., Gutierrez-Sanchez, C., Toscano, M.D., Shleev, S., De Lacey, A.L., 2013. Oxygen biosensor based on bilirubin oxidase immobilized on a nanostructured gold electrode. Bioelectrochemistry 94, 69–74.
Ricci, F., Palleschi, G., 2005. Sensor and biosensor preparation, optimisation and applications of Prussian Blue modified electrodes. Biosens. Bioelectron. 21 (3), 389–407.
Rogers, J., Huang, Y., Schmidt, O.G., Gracias, D.H., 2016. Origami MEMS and NEMS. MRS Bull. 41 (2), 123–129.
Rogers, J.A., 2017. Wearable electronics: nanomesh on-skin electronics. Nat. Nanotechnol. 12 (9), 839–840.
Rogers, J.A., Someya, T., Huang, Y., 2010. Materials and mechanics for stretchable electronics. Science 327 (5973), 1603–1607 (New York, N.Y.).
Sacks, M.S., Sun, W., 2003. Multiaxial mechanical behavior of biological materials. Annu. Rev. Biomed. Eng. 5 (1), 251–284.
Siegel, A.C., Phillips, S.T., Dickey, M.D., Lu, N., Suo, Z., Whitesides, G.M., 2010. Foldable printed circuit boards on paper substrates. Adv. Funct. Mater. 20 (1), 28–35.
Tang, Y., Yin, J., 2017. Design of cut unit geometry in hierarchical kirigami-based auxetic metamaterials for high stretchability and compressibility. Extreme Mech. Lett. 12, 77–85.
Tkac, J., Ruzgas, T., 2006. Dispersion of single walled carbon nanotubes. Comparison of different dispersing strategies for preparation of modified electrodes toward hydrogen peroxide detection. Electrochem. Commun. 8 (5), 899–903.
Wang, C., Wang, C., Huang, Z., Xu, S., 2018. Materials and structures toward soft electronics. Adv. Mater. e1801368 (Deerfield Beach, Fla.).
Webb, R.C., Bonifas, A.P., Behnaz, A., Zhang, Y., Yu, K.J., Cheng, H., Shi, M., Bian, Z., Liu, Z., Kim, Y.-S., Yeo, W.-H., Park, J.S., Song, J., Li, Y., Huang, Y., Gorbach, A.M., Rogers, J.A., 2013. Ultrathin conformal devices for precise and continuous thermal characterization of human skin. Nat. Mater. 12, 938.
Yang, Y., Gao, W., 2018. Wearable and flexible electronics for continuous molecular monitoring. Chem. Soc. Rev.
Yao, H.-B., Ge, J., Wang, C.-F., Wang, X., Hu, W., Zheng, Z.-J., Ni, Y., Yu, S.-H., 2013. A flexible and highly pressure-sensitive graphene–polyurethane sponge based on fractured microstructure design. Adv. Mater. 25 (46), 6692–6698.
Yoon, J., Jeong, Y., Kim, H., Yoo, S., Jung, H.S., Kim, Y., Hwang, Y., Hyun, Y., Hong, W.-K., Lee, B.H., Choa, S.-H., Ko, H.C., 2016. Robust and stretchable indium gallium zinc oxide-based electronic textiles formed by cilia-assisted transfer printing. Nat. Commun. 7, 11477.
Yu, K.J., Kuzum, D., Hwang, S.W., Kim, B.H., Juul, H., Kim, N.H., Won, S.M., Chiang, K., Trumpis, M., Richardson, A.G., Cheng, H., Fang, H., Thomson, M., Bink, H., Talos, D., Seo, K.J., Lee, H.N., Kang, S.K., Kim, J.H., Lee, J.Y., Huang, Y., Jensen, F.E., Dichter, M.A., Lucas, T.H., Viventi, J., Litt, B., Rogers, J.A., 2016. Bioresorbable silicon electronics for transient spatiotemporal mapping of electrical activity from the cerebral cortex. Nat. Mater. 15 (7), 782–791.
Yun, S.O., Cho, H.W., Suh, J.H., Park, J.h., Choi, B.G., Lee, T.J., Kweon, S.J., Lee, J.K., Seo, C.H., Yoo, H.J., Kim, C.Y., 2017. Flexible pH Sensor and System Fabricated Using PET Film. 2017 IEEE SENSORS, Glasgow, pp. 1–3. https://doi.org/10.1109/ICSENS.2017.8233925. http://ieeexplore.ieee.org/stamp/stamp.jsp?tp=&arnumber=8233925&isnumber=8233862.
Zhang, Y., 2016. Mechanics and designs of stretchable bioelectronics. In: Rogers, J.A., Ghaffari, R., Kim, D.-H. (Eds.), Stretchable Bioelectronics for Medical Devices and Systems. Springer International Publishing, Switzerland, pp. 53–68.
Zhang, Y., Xu, S., Fu, H., Lee, J., Su, J., Hwang, K.-C., Rogers, J.A., Huang, Y., 2013. Buckling in serpentine microstructures and applications in elastomer-supported ultra-stretchable electronics with high areal coverage. Soft Matter 9 (33), 8062–8070.